Direct constraints on diffusion models from cosmic-ray positron data: Excluding the MIN model for dark matter searches

Julien Lavalle, David Maurin, Antje Putze

Direct constraints on diffusion models from cosmic-ray positron data: Excluding the MIN model for dark matter searches

Julien Lavalle
Laboratoire Univers & Particules de Montpellier (LUPM), CNRS-IN2P3 & Université Montpellier II (UMR-5299), Place Eugène Bataillon, F-34095 Montpellier Cedex 05 — France[*]

David Maurin
LPSC, Université Grenoble-Alpes, CNRS/IN2P3, 53 avenue des Martyrs, F-38026 Grenoble — France[†]

Antje Putze
LAPTH, Université de Savoie, CNRS, B.P.110, F-74941 Annecy-le-Vieux — France [‡]

Galactic Cosmic-ray (CR) transport parameters are usually constrained by the boron-to-carbon ratio. This procedure is generically plagued with degeneracies between the diffusion coefficient and the vertical extent of the Galactic magnetic halo. The latter is of paramount importance for indirect dark matter (DM) searches, because it fixes the amount of DM annihilation or decay that contributes to the local antimatter CR flux. These degeneracies could be broken by using secondary radioactive species, but the current data still have large error bars, and this method is extremely sensitive to the very local interstellar medium (ISM) properties. Here, we propose to use the low-energy CR positrons in the GeV range as another direct constraint on diffusion models. We show that the PAMELA data disfavor small diffusion halo ($L \lesssim 3$ kpc) and large diffusion slope models, and exclude the minimal (*min*) configuration (Maurin et al. 2001, Donato et al. 2004) widely used in the literature to bracket the uncertainties in the DM signal predictions. This is complementary to indirect constraints (diffuse radio and gamma-ray emissions) and has strong impact on DM searches. Indeed this makes the antiproton constraints more robust while enhancing the discovery/exclusion potential of current and future experiments, like AMS-02 and GAPS, especially in the antiproton and antideuteron channels.

I. INTRODUCTION

The theoretical understanding of cosmic-ray (CR) transport relies on diffusion of charged particles off magnetic turbulences and has been established for decades [1–3]. In this picture, CRs are confined in an extended region that encompasses the Galactic disk, which can be assumed as a homogeneous magnetic cylinder at first order. Therein the diffusion tensor is reduced to a rigidity-dependent scalar (homogeneous and isotropic diffusion). Yet, it is only very recently that we have been able to start probing the fine structure of CR phenomenology. With the advent of space experiments like PAMELA [4–9], Fermi [10, 11], and more recently AMS-02 [12], the physics of Galactic cosmic rays (CRs) has just entered the precision era. CR measurements also provide very interesting probes of exotic physics. In particular, the survey of antimatter CR species may unveil traces of dark matter (DM) annihilation or decay in the Galaxy (*e.g.* [13–15]).

The background to DM searches mostly comes from secondary CRs, *i.e.* those CRs produced from nuclear interactions between the CR nuclei and the interstellar gas (so-called spallation). This secondary component is used to constrain the CR transport model parameters, as the ratio of secondary-to-primary CR nuclei depends very little on the properties of the primaries at their sources, while very strongly on the transport history [16, 17]. The most widely used ratio is B/C [18–25], although other ratios like ^{2}He/^{1}H and ^{3}He/^{4}He are equally powerful [26]. Once the transport parameters are set (from B/C analysis), one can fully predict the fluxes of the other secondary species provided the relevant production cross sections are known. Such calculations have been done for secondary positrons [27–30], antiprotons [31–34], and antideuterons [35]. For all but the positron case, for which energy losses play a major role in contrast to nuclei, these computations are poorly sensitive to the theoretical uncertainties affecting the transport parameters in spite of the large degeneracies induced by the B/C analysis [19, 20]. Indeed, secondary nuclei experience the same propagation history as boron nuclei.

In 2-zone diffusion models, the most critical uncertainty for DM searches stems from the degeneracy between the normalization of the diffusion coefficient[1] K_0 and half the vertical extent of the diffusion halo L. In-

[*] lavalle@in2p3.fr
[†] dmaurin@lpsc.in2p3.fr
[‡] putze@lapth.cnrs.fr

[1] We will assume $K(\mathcal{R} \equiv |p/q|) = \beta\, K_0 (\mathcal{R}/1\,\mathrm{GV})^\delta$ in the following — where p is the momentum, β the velocity, and q the electric charge.

deed, the B/C data mostly constrain the CR escape time $\propto L/K_0$ — as all other secondary-to-primary ratios of stable nuclei originating from the Galactic disk. In contrast, DM-induced CRs are produced all over the diffusion halo (and outside), and its size L has a strong impact on the signal predictions: their flux roughly scales like $\sim L^2/K_0$ (assuming a constant DM density, a fairly good approximation for qualitative understanding). This picture is valid whenever the transport is dominated by spatial diffusion.

In Ref. [36], the Authors proposed two extreme configurations to bracket the theoretical uncertainties on the DM signal predictions, dubbed *min* and *max*, relying on the B/C analysis performed in [20]. The former (latter) is featured by a very small (large) diffusion zone with $L = 1$ (15) kpc, and is associated with low (large) signal predictions. In practice, the *min* model is usually invoked to minimize the antiproton constraints on DM candidates, while *max* is used to promote detectability — the relative difference between the two almost reaches two orders of magnitude in terms of flux predictions. Such a large range for L strongly affects the antimatter CRs as reliable probes of the DM parameter space. This is particularly important in the light-intermediate WIMP mass range (10-100 GeV), where antiprotons could be used to place severe constraints on WIMPs annihilating or decaying into quarks [37].

There are serious hints that L should be larger than $\sim$1 kpc, but no stringent bounds so far. Radioactive species are insensitive to L at low energy because their lifetime is shorter than the diffusion time to reach the halo boundary. Using for instance ^{10}Be/^{9}Be breaks the K_0/L degeneracy and sets constraints on L [19, 21]. However, it was shown in several studies that this method is very sensitive to the modeling of the local interstellar medium (ISM), and strongly affected by the presence of a local underdensity, known as the *local bubble* [38, 39]: this relaxes the lower bound on L, depending on the size of the underdense region [24, 40]. There are also other, while more indirect, hints for larger values for L, coming *e.g.* from calculations of the diffuse Galactic gamma-ray [41] or radio emissions [42–44]. Nevertheless, predictions of these observables rely on more ingredients (line-of-sight integrals depending on the astrophysical source, ISM, and/or magnetic field distributions).

In this paper, we propose to use the low-energy *secondary* CR positrons as an additional direct constraint on L. We exploit the fact that the propagation history of positrons is different from that of nuclei, due to energy losses. This typically shortens the mean free path of positrons, and the dependence on L is milder. In particular, the secondary positron flux roughly scales like $\sim 1/\sqrt{K_0}$, allowing us to place a lower bound on L from the current positron data, assuming the B/C-induced relation between K_0 and L. We will only rely on secondary positrons, though it is clear that a primary component is also expected from recent measurements of the positron fraction [4, 10, 12]. Our approach, suggested in [45], is complementary to the study carried later in Ref. [44], though with a different propagation treatment, for which the main constraints came from the diffuse radio emission data. We first briefly discuss the propagation modeling and relevant parameters, then sketch our statistical analysis method, before going to the results and conclusion.

II. TRANSPORT OF COSMIC-RAY POSITRONS

We wish to constrain small 2D diffusion halo models, with typical vertical sizes of $L \sim 1$ kpc. In this context, as observers located at 8 kpc from the Galactic center but still far enough from the radial border located at a distance $\sim$ 10-15 kpc from us, we can safely neglect the radial escape. We then restrict ourselves to a much simpler 1D problem along the vertical axis. The source of secondary positrons originates in the Galactic disk from spallation processes induced by the primary cosmic rays scattering off the interstellar gas. This source term is well constrained within a radius of ~ 1 kpc around the Earth, since the cosmic-ray flux barely varies over such a spatial scale, and the average gas density confined in the disk is well estimated. It can safely be approximated to $\mathcal{Q}(E,\vec{x}) = 2\,h\,n_{\rm ism}\,\delta(z)\,Q_0(E)$, where $n_{\rm ism} = 1\,{\rm cm}^{-3}$ is the ISM gas density, $h = 100$ pc is half the disk width. The energy dependence is carried by $Q_0(E) = 4\,\pi\,n_{\rm ism}\sum_{i,j} f_j \int dT\,(d\phi_{{\rm cr,i}}(T)/dT)\,(d\sigma_{ij\to e^+}(E)/dE)$, which convolves the CR flux (species i) with the ISM gas (species j, featuring a fraction f_j).

In the following, we will stick to the formalism presented in [28–30] for the calculation of secondary positrons. In [28] (see their Fig. 10), it was shown that transport configurations implying both reacceleration and convection resulted in a prominent low-energy bump around 1 GeV in the secondary positron flux. To be conservative in our comparison with the data, we consider that positrons are only driven by spatial diffusion and energy losses. This actually significantly reduces the computational time. We can define an energy-dependent propagation scale λ from the diffusion coefficient and the energy loss term $b(E) = -dE/dt$ as follows:

$$\lambda^2(E,E_s) = 4\int_E^{E_s} dE'\,\frac{K(E')}{b(E')} \qquad (1)$$

$$= (3.56\,{\rm kpc})^2\,\frac{K_0}{10^{-2}\,{\rm kpc}^2/{\rm Myr}}\,\frac{\tau_l}{10^{16}\,{\rm s}} \times\left\{\frac{(E/E_0)^{(\delta-\alpha+1)}}{\alpha-\delta-1}\left[1-(E/E_s)^{\alpha-\delta-1}\right]\right\} \qquad (2)$$

where E ($E_s \geq E$) is the observed (injected) positron energy, and where we have used the expression $b(E) = (E_0/\tau_l)(E/E_0)^\alpha$ for the energy losses. For GeV positrons, losses are dominated by inverse Compton and synchrotron processes and the Thomson approximation holds, such that $\alpha = 2$ and $\tau_l \simeq 10^{16}$s (for $E_0 = 1$ GeV) to a very good approximation. The propagation scale λ

allows to write the Green function for the positron transport:

$$\mathcal{G}_{\rm 1D}(E, z \leftarrow E_s, z_s) = \frac{e^{-|\frac{z-z_s}{\lambda}|^2}}{b(E)\sqrt{\pi\,\lambda^2}} \overset{z,z_s\to 0}{\longrightarrow} \frac{1}{b(E)\sqrt{\pi\,\lambda^2}} \quad (3)$$

For small-L models, one has to account for the boundary effect. When both the observer and the source term are confined into the disk ($z, z_s = 0$), the following series expansions can be used in the regime $\lambda \gtrsim L$, most relevant in the low energy range [46]:

$$\begin{aligned}\mathcal{G}_{\rm 1D,Helm}(E \leftarrow E_s) &= \frac{1}{b(E)\,L}\sum_{n=1}^{n=+\infty} e^{-|\frac{(2\,n-1)\,\lambda}{4\,L}|^2} \quad (4)\\ &\approx \frac{e^{-|\frac{\lambda}{4\,L}|^2} + e^{-|\frac{3\,\lambda}{4\,L}|^2}}{b(E)\,L}\,,\end{aligned}$$

If we express the B/C correlation between K_0 and L as $K_0 = \kappa\,L$, with $\kappa \sim 10^{-3}$ kpc/Myr [20], we can read off the dependence of the CR positron density on L from the leading term of the series:

$$\mathcal{G}_{\rm 1D,Helm}(E \leftarrow E_s) \approx \frac{e^{-|\kappa\,\tau_l\,f(E,E_s)|^2}}{b(E)\,L}\,,$$

where $f(E, E_s) \approx (E/E_0)^{(\delta-1)}/(1-\delta) \approx 2\sqrt{E/({\rm GeV})}$. Interestingly, the exponential term no longer depends on K_0 and L (because of the cancellation in the ratio $\lambda/L \propto K_0/L \propto \kappa$), and the leading pre-factor is therefore proportional to $1/(b(E)\,L)$, where it appears clearly that small values of L lead to large secondary positron fluxes.

So far, we have mostly discussed the roles of K_0 and L. The impact of δ can be understood from the predicted spectral shape for the secondary positron flux [29], which roughly scales as $E^{-\tilde{\gamma}}$, with the spectral index $\tilde{\gamma} \simeq \gamma + (1+\delta)/2$, where $\gamma \approx 2.7$ is the source index associated with secondary positron production. Therefore, the smaller δ the harder the secondary positron spectrum.

Finally, we also emphasize that since we focus on the GeV energy range, our results are sensitive to solar modulation effects. We use the one-parameter force-field model [47] to take it into account, and discuss its effects into more details afterward.

III. STATISTICAL ANALYSIS

Given the measured positron flux $\phi_{\rm data}(E)$ and associated statistical error $\sigma_{\phi_{\rm data}}(E)$, we wish to constrain *only* those transport models which lead to secondary positron fluxes *in excess* with respect to the data. For each data point at kinetic energy E_i, the number of standard deviations in a one-sided hypothesis test of a Gaussian variate, *i.e.* the Z-score, is calculated:

$$Z_i = \frac{\phi_{\rm model}(E_i) - \phi_{\rm data}(E_i)}{\sigma_{\phi_{\rm data}}(E_i)}\,, \quad (5)$$

where $\phi_{\rm model}(E_i)$ is the modulated flux estimated for a given parameter set $\{K_0,\ L,\ \delta\}$. In a subsequent step, the individual p-value p_i is estimated only for data points with a positive Z_i:

$$p_i = 1 - \Phi(Z_i) = \frac{1 - {\rm erf}(Z_i/\sqrt{2})}{2}\,, \quad (6)$$

where $\Phi(Z)$ is the cumulative distribution function of the Gaussian distribution. The independent p_i values of a given model are eventually combined into a single test statistic X using Fisher's method [48]:

$$X = -2\sum_i^n \log p_i\,. \quad (7)$$

X follows closely a χ^2_{2n} with $2n$ degrees of freedom from which a p-value for the global hypothesis can be easily obtained:

$$p = 1 - \frac{\gamma(n, \chi^2_{2n}/2)}{\Gamma(n)}, \quad (8)$$

where γ and Γ are the lower incomplete and complete gamma functions, respectively.

In the following, we will use a 3-σ exclusion criterion of $p < 0.001345$, which corresponds to excluding only models that exceed the data by 3-σ or more.

IV. RESULTS AND DISCUSSION

For the predictions of the secondary positron flux, we use the framework defined in [28, 29] and associated energy loss parameters. As we disregard reacceleration and convection, a transport model is defined by the normalization of the diffusion coefficient K_0, its slope δ, and the halo height L, that we vary in the ranges $K_0/L \in [10^{-3}, 10^{-2}]$ kpc/Myr, $\delta \in [0.2\text{-}0.9]$, consistent with the B/C constraints [20].

To cover the great variety of possible diffusion model parameters found in the literature, 500 000 parameter sets have been uniformly drawn in the ranges defined above. We have used the PAMELA data [9] associated with a reference solar modulation potential of 520 MV taken from the recent analysis in Ref. [49], and corresponding to the data taking period. We also checked our method with the unpublished AMS-02 data presented at ICRC 2013 (and available from online plots), but will only comment on the trend waiting for the AMS-02 collaboration to confirm their results. A 2D projection in the $\log(K_0/L)$–L plane of (i) the models parameters drawn, (ii) those leading to positron fluxes not exceeding the PAMELA data ($\forall\ i : Z_i \leq 0$), and (iii) those leading to positron fluxes in excess with respect to one or more data points ($\exists\ i\ :\ Z_i > 0$), are shown in left, middle, and right panel of Fig. 1, respectively. The AMS-02 data from ICRC 2013 would lead to the same trends. It can already be seen that the secondary positrons constrain

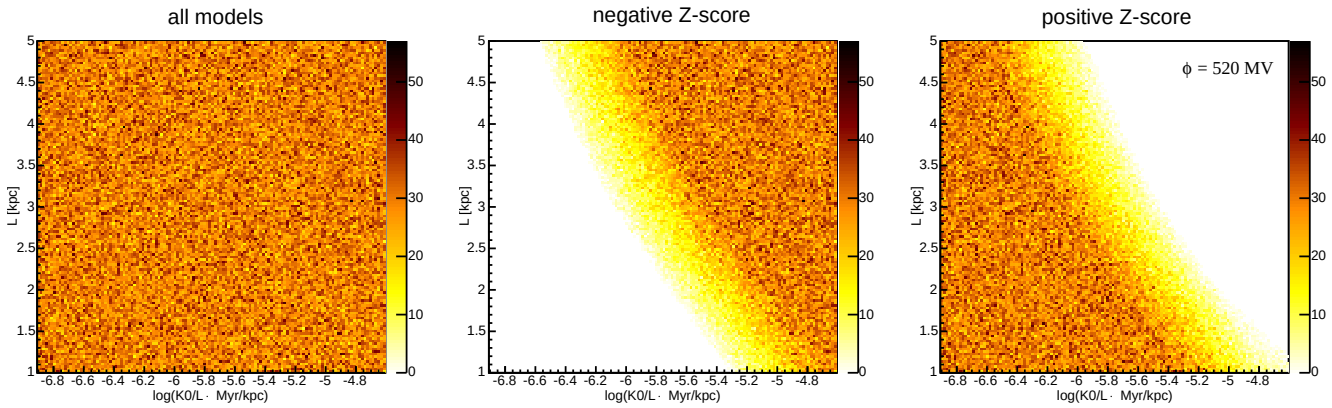

FIG. 1: 2D histograms for L versus $\log(K_0/L)$ for $\delta \in [0.2\text{-}0.9]$.

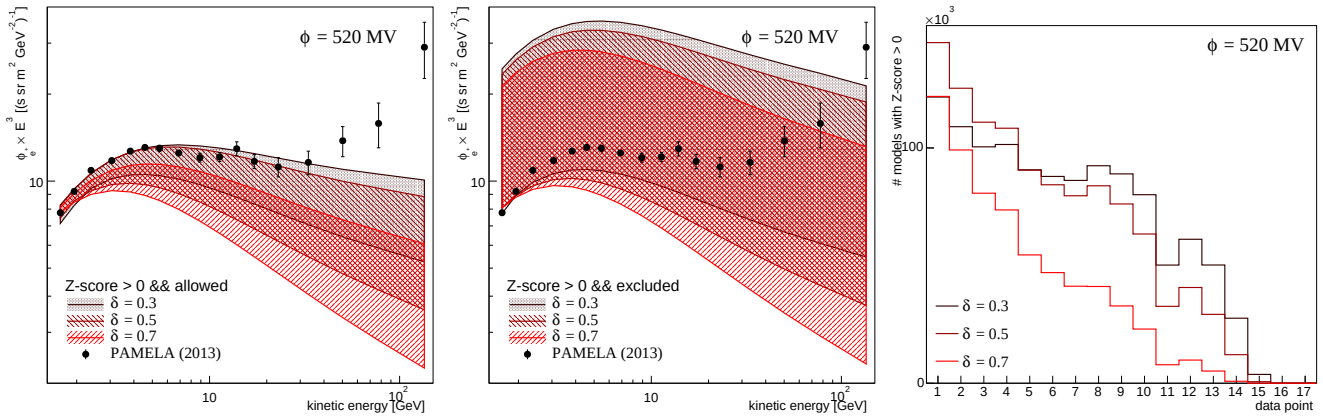

FIG. 2: Left: contours of the secondary positron flux predictions in excess with one or more data points, still allowed by our analysis. Middle: the same for models excluded by our analysis. Right: histogram of the data points leading to $Z_i > 0$, for the excluded transport models.

extensively low values of L and $\log(K_0/L)$ independent of the spectral index δ (white area in the middle plot).

The influence of the slope δ can be understood from Fig. 2. In the left (middle) panel, we show the predicted fluxes associated with $Z > 0$ while not excluded (excluded) by our analysis, for different slices in δ (the $Z < 0$ models, not shown here, give fluxes that spread over a large area below the data points). We see that the larger δ, the more important the constraint from low-energy data points, as it can be expected from the flux dependence in δ (see Sec. II). In contrast, fluxes predicted from a more gradual slope of $\delta \sim 0.3$ follow the experimental data more closely (in the GeV range) and are hence equally constrained by the PAMELA data points 1 to 14 ranging from 1.64 to 33.1 GeV. In the right panel of Fig. 2, we display the data points which have individual positive Z-score ($Z_i > 0$) for the models excluded from our nominal analysis, for different slices in δ. The trend explained above is explicit in this plot.

In Fig. 3, we show the 3-σ exclusion curves we obtain in the $\log(K_0/L) - L$ plane. This is the main result of this paper. Plain lines correspond to the exclusion curves

	δ	K_0	L	V_c	V_A
	-	(kpc^2 Myr^{-1})	(kpc)	(km s^{-1})	(km s^{-1})
max	0.46	0.0765	15	5	117.6
med	0.70	0.0112	4	12	52.9
min	0.85	0.0016	1	13.5	22.4

TABLE I: Transport parameters (compatible with the B/C analysis) giving the *max*, *med* and *min* $\bar{p}$ and $\bar{d}$ dark matter flux.

associated with different values of δ. Dashed lines show how the results are changed if the secondary positron flux predictions are increased by a global factor of 30%, a very rough way to account for a possible contamination of primary positrons at low energy. In the top panels, we adopt nominal values for the solar modulation, *i.e.* 520 MV for the PAMELA data taking period, and use all data points to compute the Z-score. In the bottom panel, we take a very conservative viewpoint to secure the results against systematic effects potentially coming from the solar modulation modeling or any other low energy effects, (i) by imposing an analysis threshold of ∼2 GeV

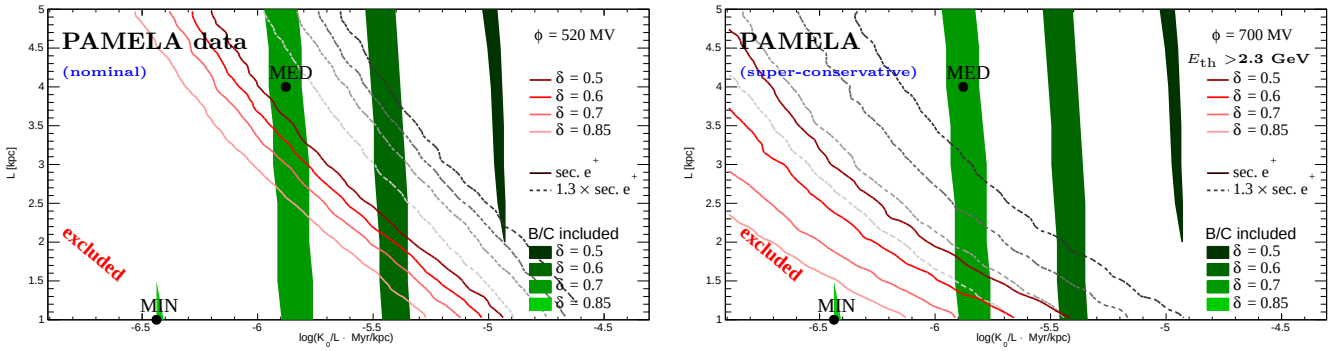

FIG. 3: Constraints on propagation parameters in the $\log(K_0/L$ in [kpc/Myr]$)$-L [kpc] plane. Lines are constraints from the positron flux (separating excluded and allowed regions). Green filled contours are allowed by B/C data. The *min* and *med* benchmark models of Ref. [36] (see Tab. I) are indicated by a filled black circle. **Left panel:** positron contours (from PAMELA data) for a realistic modulation level of $\phi = 520$ MV. Dashed lines correspond to the limits if the secondary positron prediction is increased by 30% to mimic a primary component. **Bottom panel (very conservative):** Same contours but for a modulation level larger than observed, 700 MV, and taking a very conservative analysis threshold of ∼2 GeV.

(lower energy data points are not considered), and (ii) by significantly increasing the solar modulation parameter ϕ up to 700 MV.

We report on the same plots the constraints set from B/C as obtained in [20], in the form of bands corresponding to different diffusion slopes δ. There are several reasons as for why most recent studies are not used. First, although powerful statistical tools have been employed since [24–26] to sample the most probable regions of the parameter space, we are interested in a wider and more conservative range such as given in [20]. This allows us to include possible systematic uncertainties on the transport parameters that plague their precise determination [24]. Second, the benchmark models (*min*, *med*, *max*) of Ref. [36], widely used in the literature, are based on the parameters found in Ref. [20]. We have placed the points corresponding to the *min* and *med* models in both panels of Fig. 3, while the *max* model is featured by a too large value of $L = 15$ kpc, outside the scope of this paper. Each point belongs to a B/C band associated with a given slice in δ. The detailed values of the parameters are given in Table I.

An important feature of Fig. 3 is that the positron and B/C constraints are almost orthogonal in the $\log(K_0/L)$-L plane, underlying their complementarity. This is definitely a strength of this approach as it can complement the one relying on radioactive species, which has completely different systematics. We first concentrate on the left panel, which shows our nominal result. As we can see, the *min* model is completely excluded. This is an important result per se because this model is very often used in the literature to deal with the theoretical uncertainties affecting the dark matter signal predictions. More generally, models with large values of δ (~ 0.8), generically associated with small diffusion halos ($L \sim 1$ kpc), are excluded by our analysis. Smaller values of δ are featured by larger K_0/L ratios. For example, we see that for the B/C band that contains the *med* model ($\delta \sim 0.7$), the positron data exclude diffusion halos with $L \lesssim 3$ kpc, while a less severe constraint of $L \lesssim 2.3$ is obtained for smaller diffusion slopes. The dashed lines indicate how these limits would move if a primary positron component contributed an additional 30% to the positron flux at low energy, leading to much larger values of L. Nevertheless, though we know that a primary component is present in the positron data, its origin is still to be confirmed, and its intensity at low energy can hardly be predicted. We emphasize that the local positron flux provides a *direct* constraint, which relies on less assumptions (*e.g.* on the distribution of the Galactic magnetic field or the interstellar radiation field) than, for example, limits set from the diffuse radio and gamma-ray emissions, where electrons and positrons are also strongly involved.

We remind the reader that we have already followed a conservative line by neglecting diffusive reacceleration, which would have increased our predictions around 1.5-2 GeV as δ decreases [28]; we have also neglected any primary component. We can still investigate further the systematic effects. As we deal with low-energy positrons, the exact value of the solar modulation level has significant impact on the limit derived, as well as its modeling. The force-field approximation is known to be a simplistic modeling of the solar modulation, but is expected to be accurate within ∼10-20% above 100 MeV [50]. In our nominal analysis, we took a modulation potential of 520 MV, and exploited all PAMELA data points down to 1.64 GeV — the lowest energy data points have strong impact on large δ propagation models. In order to check our results against systematic effects, we adopt the radical option to (i) increase the modulation potential up to 700 MeV and (ii) to remove the first two data points from the analysis, setting a threshold at ∼2 GeV (more

precisely 2.38 GeV, 3rd PAMELA data point). Such an option is extreme, so the corresponding results are to be taken as super-conservative. They are displayed in the right panel of Fig. 3. The limits on L are generically weaker, but the *min* model remains excluded, as propagation models with large values of δ (~ 0.8).

V. CONCLUSION

In this paper, we have investigated the low-energy positron constraints ($\lesssim 10$ GeV) on 2-zone cosmic-ray propagation models. We have shown that the resulting bounds are almost orthogonal to the B/C constraints in the L-log(K_0/L) plane, which makes them particularly attractive. The main result is that we exclude the *min* benchmark propagation model and more generally large diffusion indices δ ($\gtrsim 0.8$). We also strongly disfavor small diffusion halo models with $L \lesssim 3$ kpc, the constraint weakening as the diffusion slope δ decreases. This has important consequences for dark matter studies which are often addressed in the frame of 2-zone models. Indeed, this pushes the DM signal predictions toward larger values, which has significant impact on the discovery/exclusion potential of current and future experiments. This will be of particular interest for the searches in the antiproton and antideuteron channels, with AMS-02 and GAPS [51–53].

The strength of the proposed analysis, complementary to the B/C or radioactive studies, will significantly improve when the AMS-02 data are released (more data points with smaller error bars). Preliminary calculations based on the preliminary AMS-02 data presented at the ICRC-2013 conference already give slightly stronger constraints on L. The next step of this work, that we currently prepare, will be to implement a full study including all low-energy effects and combining the coming AMS-02 data on positrons and PAMELA and AMS-02 data on B/C.

We note that the PAMELA collaboration has just released its B/C data [54]. With an analysis based on a very limited number of parameters, the Authors constrain the diffusion slope δ to be in the range $\sim [0.38 - 0.42]$. However, the choice of the free parameters (wind or no wind, low energy dependence of the diffusion coefficient) has a strong impact on the result, and in particular on δ [24, 55]. It is important to perform a full scan of the parameter space with these new B/C data (awaiting for the AMS-02 positron data and final B/C analysis). Better constraints on δ should increase the discrimination power of positrons.

ACKNOWLEDGMENTS

We would like to thank L. Derome for useful discussions about statistical analysis methods. This work was partly funded by the French ANR, *Programme BLANC* DMAstro-LHC, Project ANR-12-BS05-0006, and by the *Investissements d'avenir, Labex ENIGMASS*.

1 V. S. Berezinskii *et al.*, *Astrophysics of cosmic rays* (Amsterdam: North-Holland, edited by Ginzburg, V.L., 1990).
2 R. Schlickeiser, *Cosmic ray astrophysics* (Springer Berlin Heidelberg, 2002).
3 A. W. Strong *et al.*, Annual Review of Nuclear and Particle Science **57**, 285 (2007), astro-ph/0701517.
4 O. Adriani *et al.*, Nature **458**, 607 (2009), arXiv:0810.4995.
5 O. Adriani *et al.*, Phys. Rev. Lett. **105**, 121101 (2010), arXiv:1007.0821 [astro-ph.HE].
6 O. Adriani *et al.*, Science **332**, 69 (2011), arXiv:1103.4055 [astro-ph.HE].
7 O. Adriani *et al.*, Phys. Rev. Lett. **106**, 201101 (2011), arXiv:1103.2880 [astro-ph.HE].
8 O. Adriani *et al.*, Astrophys. J. **770**, 2 (2013), arXiv:1304.5420 [astro-ph.HE].
9 O. Adriani *et al.*, Phys. Rev. Lett. **111**, 081102 (2013).
10 A. A. Abdo *et al.*, Phys. Rev. Lett. **102**, 181101 (2009), arXiv:0905.0025.
11 M. Ackermann *et al.*, Phys. Rev. Lett. **108**, 011103 (2012), arXiv:1109.0521 [astro-ph.HE].
12 M. Aguilar *et al.*, Phys. Rev. Lett. **110**, 141102 (2013).
13 J. Silk and M. Srednicki, Physical Review Letters **53**, 624 (1984).
14 T. A. Porter, R. P. Johnson, and P. W. Graham, Ann.Rev.Astron.Astrophys. **49**, 155 (2011), arXiv:1104.2836 [astro-ph.HE].
15 J. Lavalle and P. Salati, Comptes Rendus Physique **13**, 740 (2012), arXiv:1205.1004 [astro-ph.HE].
16 D. Maurin, R. Taillet, and F. Donato, Astron.Astroph. **394**, 1039 (2002), astro-ph/0206286.
17 A. Putze, D. Maurin, and F. Donato, Astron.Astroph. **526**, A101 (2011), arXiv:1011.0989 [astro-ph.GA].
18 W. R. Webber, M. A. Lee, and M. Gupta, Astrophys. J. **390**, 96 (1992).
19 F. C. Jones, A. Lukasiak, V. Ptuskin, and W. Webber, Astrophys. J. **547**, 264 (2001), astro-ph/0007293.
20 D. Maurin, F. Donato, R. Taillet, and P. Salati, Astrophys. J. **555**, 585 (2001), astro-ph/0101231.
21 A. W. Strong and I. V. Moskalenko, Advances in Space Research **27**, 717 (2001), astro-ph/0101068.
22 A. M. Lionetto, A. Morselli, and V. Zdravkovic, JCAP **0509**, 010 (2005), astro-ph/0502406.
23 C. Evoli, D. Gaggero, D. Grasso, and L. Maccione, JCAP **10**, 018 (2008), arXiv:0807.4730.
24 A. Putze, L. Derome, and D. Maurin, Astron.Astrophys. **516**, A66 (2010), arXiv:1001.0551 [astro-ph.HE].
25 R. Trotta, G. Johannesson, I. Moskalenko, T. Porter, R. R. de Austri, *et al.*, Astrophys.J. **729**, 106 (2011), arXiv:1011.0037 [astro-ph.HE].
26 B. Coste, L. Derome, D. Maurin, and A. Putze, Astron.Astroph. **539**, A88 (2012), arXiv:1108.4349 [astro-ph.GA].
27 I. Moskalenko and A. Strong, Astrophys.J. **493**, 694

(1998), astro-ph/9710124.
28 T. Delahaye, R. Lineros, F. Donato, N. Fornengo, J. Lavalle, P. Salati, and R. Taillet, Astron.Astrophys. **501**, 821 (2009), arXiv:0809.5268.
29 T. Delahaye, J. Lavalle, R. Lineros, F. Donato, and N. Fornengo, Astron.Astrophys. **524**, A51 (2010), arXiv:1002.1910 [astro-ph.HE].
30 J. Lavalle, Mon.Not.Roy.Astron.Soc. **414**, 985L (2011), arXiv:1011.3063 [astro-ph.HE].
31 F. Donato, D. Maurin, P. Salati, A. Barrau, G. Boudoul, and R. Taillet, Astrophys. J. **563**, 172 (2001), astro-ph/0103150.
32 T. Bringmann and P. Salati, Phys.Rev. **D75**, 083006 (2007), astro-ph/0612514.
33 F. Donato, D. Maurin, P. Brun, T. Delahaye, and P. Salati, Phys. Rev. Lett. **102**, 071301 (2009), arXiv:0810.5292.
34 G. Di Bernardo, C. Evoli, D. Gaggero, D. Grasso, and L. Maccione, Astroparticle Physics **34**, 274 (2010), arXiv:0909.4548 [astro-ph.HE].
35 F. Donato, N. Fornengo, and D. Maurin, Phys.Rev. **D78**, 043506 (2008), arXiv:0803.2640.
36 F. Donato, N. Fornengo, D. Maurin, P. Salati, and R. Taillet, Phys. Rev. D **69**, 063501 (2004), astro-ph/0306207.
37 J. Lavalle, Phys.Rev. **D82**, 081302 (2010), arXiv:1007.5253 [astro-ph.HE].
38 R. Lallement, B. Y. Welsh, J. L. Vergely, F. Crifo, and D. Sfeir, Astron.Astroph. **411**, 447 (2003).
39 R. Lallement, J.-L. Vergely, B. Valette, L. Puspitarini, L. Eyer, and L. Casagrande, Astron.Astroph. **561**, A91 (2014), arXiv:1309.6100 [astro-ph.GA].
40 F. Donato, D. Maurin, and R. Taillet, Astron.Astrophys. **381**, 539 (2002), astro-ph/0108079.
41 M. Ackermann *et al.*, Astrophys. J. **750**, 3 (2012).
42 E. Orlando and A. Strong, Mon.Not.Roy.Astron.Soc. **436**, 2127 (2013), arXiv:1309.2947 [astro-ph.GA].
43 T. Bringmann, F. Donato, and R. A. Lineros, JCAP **1201**, 049 (2012), arXiv:1106.4821 [astro-ph.GA].
44 G. Di Bernardo, C. Evoli, D. Gaggero, D. Grasso, and L. Maccione, JCAP **3**, 036 (2013), arXiv:1210.4546 [astro-ph.HE].
45 J. Lavalle, J.Phys.Conf.Ser. **375**, 012032 (2012), arXiv:1112.0678 [astro-ph.HE].
46 J. Lavalle, J. Pochon, P. Salati, and R. Taillet, Astron.Astrophys. **462**, 827 (2007), astro-ph/0603796.
47 L. J. Gleeson and W. I. Axford, Astrophys. J. **154**, 1011 (1968).
48 R. A. Fisher, *Edinburgh: Oliver and Boyd, 1970, 14th ed.* (1970).
49 D. Maurin, A. Cheminet, L. Derome, A. Ghelfi, and G. Hubert, Adv.Space Res. in press (2014), 10.1016/j.asr.2014.06.021, arXiv:1403.1612 [astro-ph.EP].
50 M. Potgieter, Living Reviews in Solar Physics **10**, 3 (2013), arXiv:1306.4421 [physics.space-ph].
51 C. J. Hailey *et al.*, Advances in Space Research **51**, 290 (2013).
52 T. Aramaki *et al.*, Astroparticle Physics **59**, 12 (2014), arXiv:1401.8245 [astro-ph.HE].
53 P. von Doetinchem *et al.*, Astroparticle Physics **54**, 93 (2014), arXiv:1307.3538 [astro-ph.IM].
54 O. Adriani *et al.*, ArXiv e-prints (2014), arXiv:1407.1657 [astro-ph.HE].
55 D. Maurin, A. Putze, and L. Derome, Astron.Astroph. **516**, A67 (2010), arXiv:1001.0553 [astro-ph.HE].